Supporting Information for

Asymmetrically-channeled two-dimensional membrane for stable, selective lithium-ion transport

Meiqi Kan, Qin Huang, Lei Xu, Ying Dai, Lei Dong*

Experimental Section

Materials Synthesis: The large-sized GO nanosheets was prepared in accordance with our previous report[1]. A colloidal suspension of TiO_2 nanosheets was prepared via the exfoliation of layered titanate crystals[2]. Typically, TiO_2, K_2CO_3, and Li_2CO_3 were mixed at a molar ratio of 1.73:0.4:0.14 and calcined at a high temperature of 1100 °C for 10 hours. The obtained layered titanate ($K_{0.8}Ti_{1.73}Li_{0.27}O_4$) was then stirred in a 0.5 M HCl solution at room temperature for 24 hours. Then the acid-exchanged titanate ($H_{1.07}Ti_{1.73}O_4 \cdot H_2O$) was collected by filtration, washed with deionized water, and air-dried at room temperature. Subsequently, the protonated titanate crystals were treated by shaking in a tetrabutylammonium hydroxide ($(C_4H_9)_4NOH$, hereinafter referred to as TBAOH) solution, where the molar ratio of TBAOH concentration to the exchangeable protons in the titanate was 2:1. After standing for 7 days, the mixture was centrifuged at 10,000 rpm for 30 min, and the supernatant was collected to obtain a stable TiO_2 nanosheets dispersion.

MnO_2 nanosheets was obtained by exfoliating layered potassium birnessite (K-MnO_2)[3]. Typically, 1 g of K-MnO_2 was dispersed in 250 mL of 0.5 mol L^{-1} $(NH_4)_2S_2O_8$ solution and stirred at 60 °C for 3 h. The solid was collected after filtration. After repeating the processes, protonated MnO_2 (denoted as H-MnO_2) was obtained. Subsequently, 0.1 g of H-MnO_2 was mixed with 25 mL of tetramethylammonium hydroxide (TMAOH) aqueous solution and stirred for 2 days, where the TMAOH concentration was adjusted to 30 equivalents relative to the exchangeable H^+ in H-MnO_2. The resulting mixture was repeatedly washed and centrifuged at 6000 rpm until the supernatant became neutral, yielding TMA^+-intercalated MnO_2 (TMA-MnO_2). Likewise, TMA-MnO_2 was mixed with 25 mL of TBAOH and stirred for 10 days, giving TBA^+-intercalated MnO_2 (TBA-MnO_2) solution. Finally, after treated by ultrasonic for 30 min, the obtained solution was centrifuged

at 12000 rpm to collect the supernatant, which was transferred to a dialysis bag immersed in deionized water for dialysis (≥7 days) to remove excess TBAOH, obtaining stable MnO_2 nanosheets dispersion.

Membrane Preparation: Two types of asymmetric-channel membranes were fabricated using an identical strategy based on the hypothetical area-matching model (one GO layer paired with one TiO_2 layer). Typically, the GO-TiO_2 membrane was prepared by dropwise mixing GO and TiO_2 nanosheet dispersions at a predetermined mass ratio of 1:2.8 under continuous stirring for self-assembly, followed by vacuum filtration and drying. The GO-MnO_2 membrane was synthesized via the same assembly and post-treatment procedures, with the only variation being the use of GO and MnO_2 nanosheet dispersions mixed at a preset mass ratio of 1:2.5. Both membranes were supported on hydrophilic nylon substrates.

Membrane Characterization: XRD measurements were performed on a Bruker D8 Advance diffractometer employing Cu Kα radiation (λ = 1.5418 Å). AFM characterization was conducted using a Bruker Dimension Icon instrument to examine the morphology of the nanosheets deposited on silicon wafer and mica substrates. SEM images were recorded with a ZEISS Sigma 300 scanning electron microscope. TEM observations were carried out on a JEOL JEM-F200 transmission electron microscope. The zeta potential of the nanosheet suspension was determined using a Zetasizer Nano laser dynamic light scattering analyzer. The absorption spectrum of the nanosheet suspension was measured with a LAMBDA 365 UV-Vis spectrophotometer. Inductively coupled plasma optical emission spectrometry (ICP-OES) analyses were performed on an ICAP PRO X spectrometer. Ion permeation performance was tested using a TQ-FO100-Z forward osmosis experimental device and a homemade H-type cell setup.

Membrane Performance Test: Membrane performance was evaluated in terms of cation permeability. The ion permeability (J_a, $mol \cdot m^{-2} \cdot h^{-1}$) can be calculated using Equation (1):

$$J_a = \frac{V * (C_1 - C_0)}{A * t} \#(1)$$

Herein, V denotes the solution volume on the permeate side (unit: L); C_1 represents the current ion concentration in the permeate solution (unit: $mol \cdot L^{-1}$), and C_0 is the initial ion concentration in the permeate solution (unit: $mol \cdot L^{-1}$); A stands for the effective membrane area (unit: m^2); t is the permeation time (unit: h). Owing to the low ion concentration in the permeate solution (dilute

solution), the ionic conductivity of the solution can be converted to the ion concentration via Equation (2), and the conversion formula is as follows:

$$C = \frac{1000\kappa}{\Lambda_m} \#(2)$$

Herein, C is the ion concentration in the solution (unit: mol·L^{-1}); κ denotes the ionic conductivity of the solution on the permeate side (unit: S·m^{-1}); and Λ_m represents the molar conductivity (unit: S·m^2·mol^{-1}). The ideal separation factor (selectivity) of the single-ion system can be calculated using Equation (3):

$$a_{ab} = \frac{J_a}{J_b} \#(3)$$

In mixed ion systems, the ion concentration was measured via ICP-OES to calculate the permeability, and the corresponding calculation formula is as follows:

$$J_{M_a} = \frac{V * (\rho_1 - \rho_0)}{A * t} \#(4)$$

$$J_a = \frac{P_{M_a}}{M_a} \#(5)$$

Herein, J_{Ma} denotes the ion mass permeation rate (unit: g·m^{-2}·h^{-1}); J_a represents the ion molar permeation rate (unit: mol·m^{-2}·h^{-1}); ρ_1 is the current ion mass concentration (unit: mg·L^{-1}), and ρ_0 refers to the initial ion mass concentration (unit: mg·L^{-1}); V stands for the solution volume on the permeate side (unit: L); M_a denotes the molar mass of the ion (unit: g·mol^{-1}); A is the effective membrane area (unit: m^2); and t represents the permeation time (unit: h). Specifically, the separation factor (selectivity) of the dual-ion system can be calculated using Equation (6):

$$\beta_{ab} = \frac{J_{M_a}}{J_{M_b}} = \frac{P_{M_a}}{P_{M_b}} * \frac{M_a}{M_b} \#(6)$$

The single-ion permeability test was performed using a forward osmosis (FO) system (as shown in Figure S16), with both the feed solution and permeate solution operating in cross-flow mode. Mass transfer between the feed side and permeate side could only occur through the target membrane installed in the membrane cell. The circulation of the feed and permeate solutions was driven by two peristaltic pumps with adjustable power; the flowing liquid disturbed the boundary layer to promote uniform solution composition, thereby minimizing osmotic pressure loss caused by external concentration polarization. Taking the Li^+ single-ion permeation test as an example: equal volumes of 0.1 mol/L LiCl aqueous solution (400 mL) and deionized water (400 mL) were

added to the beakers on the feed side and permeate side, respectively. The tests were conducted using a membrane with an effective diameter of 1 cm. A digital balance was used to monitor mass changes of the solution on the permeate side, while a conductivity meter tracked variations in ionic conductivity of the permeate-side solution.

The mixed-ion permeability test was conducted via a self-fabricated H-type electrolytic cell for liquid filtration measurements (as shown in Figure S17). Equal volumes of 0.1 mol/L mixed salt solution (LiCl, NaCl, $MgCl_2$, KCl) and deionized water were added to the feed side and permeate side, respectively, with continuous stirring maintained using a magnetic stirrer. The salt content in the permeate was determined by ICP-OES.

Theoretical Calculations: DFT calculations were performed using the Vienna Ab initio Simulation Package (VASP)[4]. The exchange-correlation potential was characterized by the Perdew-Burke-Ernzerhof (PBE) formulation of the generalized gradient approximation (GGA)[5]. Electron-ion interactions were treated using the projector augmented wave (PAW) method[4]. All DFT calculations employed a cutoff energy of 400 eV, with Brillouin zone integration sampled via a 3×3×1 Monkhorst-Pack k-point grid. Van der Waals interactions were accounted for using the DFT-D3 method[5]. Subsequently, the diffusion barriers of Li^+ and Mg^{2+} ions along their respective diffusion pathways were calculated using the climbing image nudged elastic band (CI-NEB) approach.

[1] L. Dong, Z. Chen, S. Lin, C. Ma, H. Lu, *Chem. Mater.* **2017**, 29, 564.

[2] T. Sasaki, M. Watanabe, H. Hashizume, H. Yamada, H. Nakazawa, *J. Am. Chem. Soc.* **1996**, 118, 8329.

[3] P. Xiong, R. Ma, N. Sakai, X. Bai, S. Li, T. Sasaki, *ACS Appl. Mater. Interfaces.* **2017**, 9, 6282.

[4] G. Kresse, J. Hafner, *Phys. Rev. B.* **1993**, 47, 558.

[5] J. P. Perdew, K. Burke, M. Ernzerhof, *Phys. Rev. Lett.* **1996**, 77, 3865.

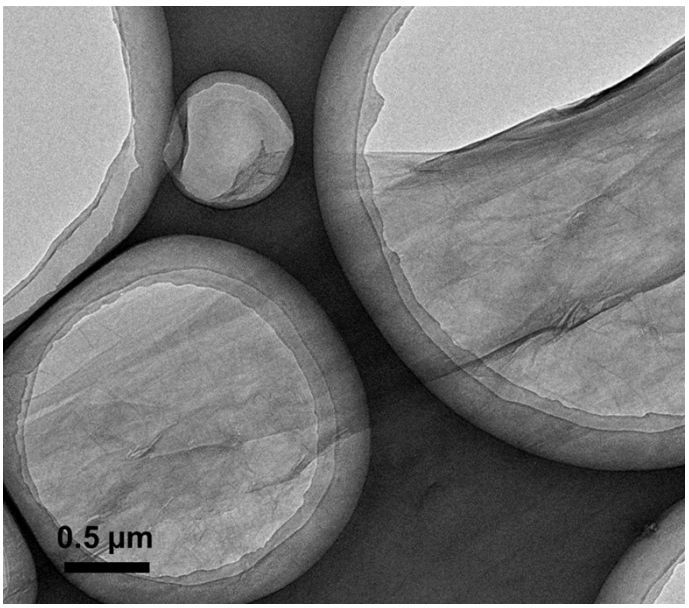

Figure S1. TEM image of large-sized GO (LGO) nanosheets

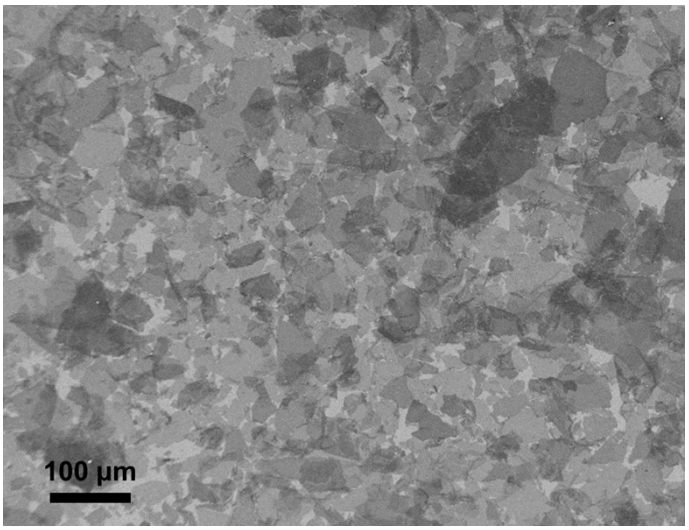

Figure S2. SEM image of LGO nanosheets. The average size is calculated to be ~67 µm

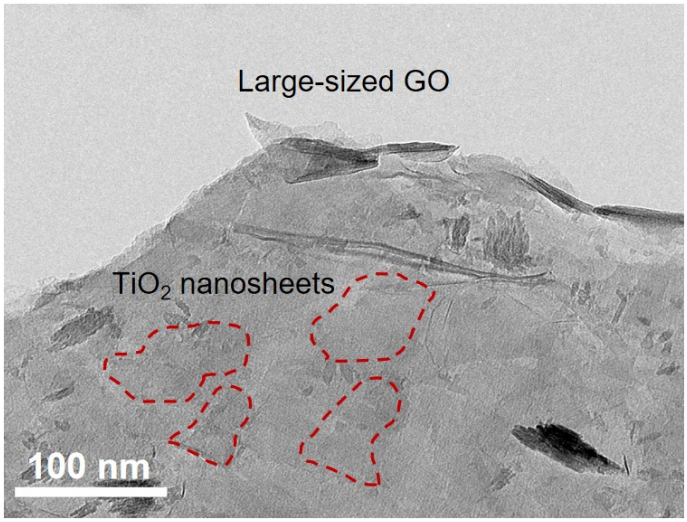

Figure S3. TEM image of the exfoliated GO-TiO_2 membrane. Small TiO_2 nanosheets (marked by red dot-lines) are loaded onto the large-sized GO

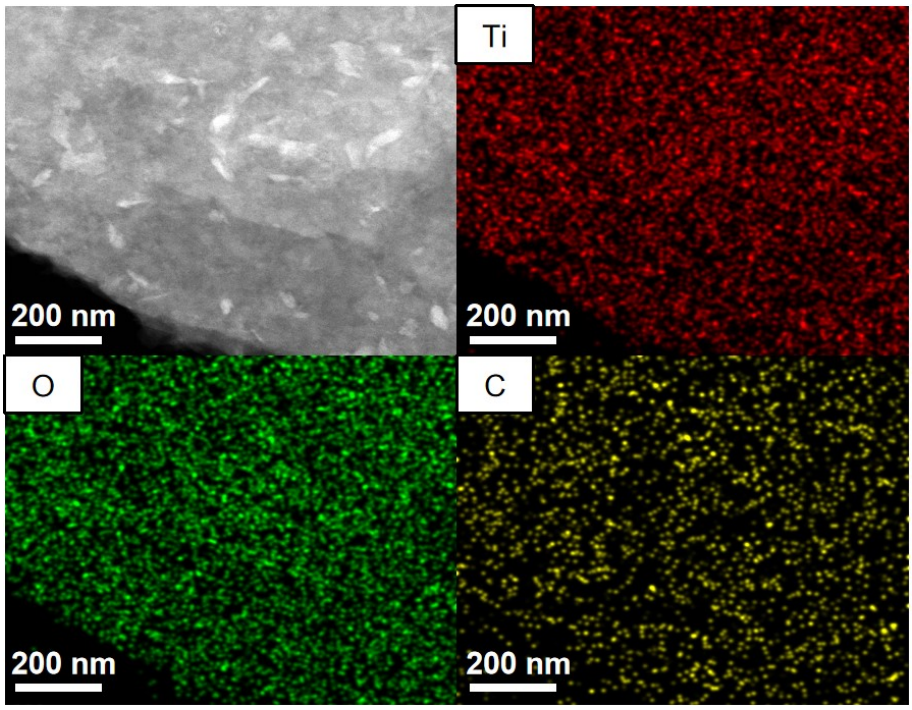

Figure S4. TEM image (top-left) and the corresponding elemental distribution mapping of GO-TiO_2 membrane.

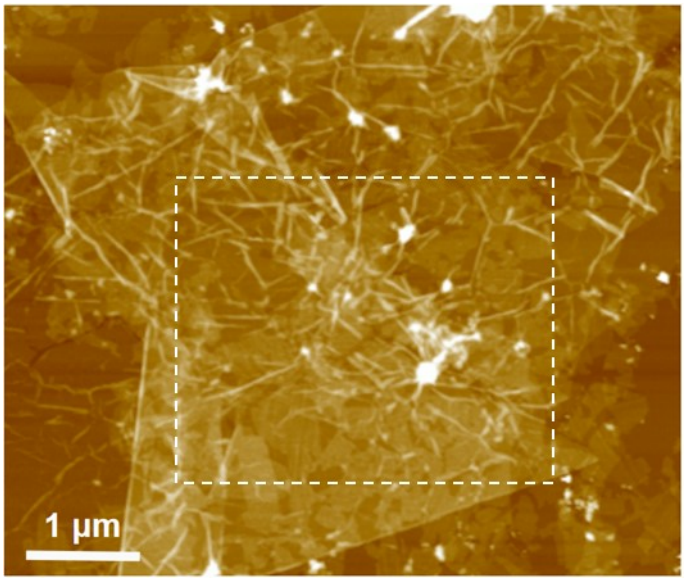

Figure S5. AFM image of the multi-layered GO-TiO_2. The roughness (selected area) is measured to be 1.68 nm

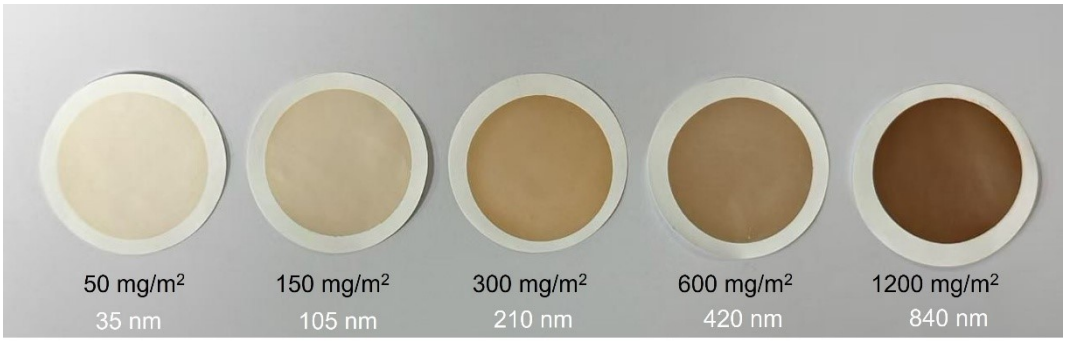

Figure S6 Photographs of GO-TiO_2 membranes with different thicknesses.

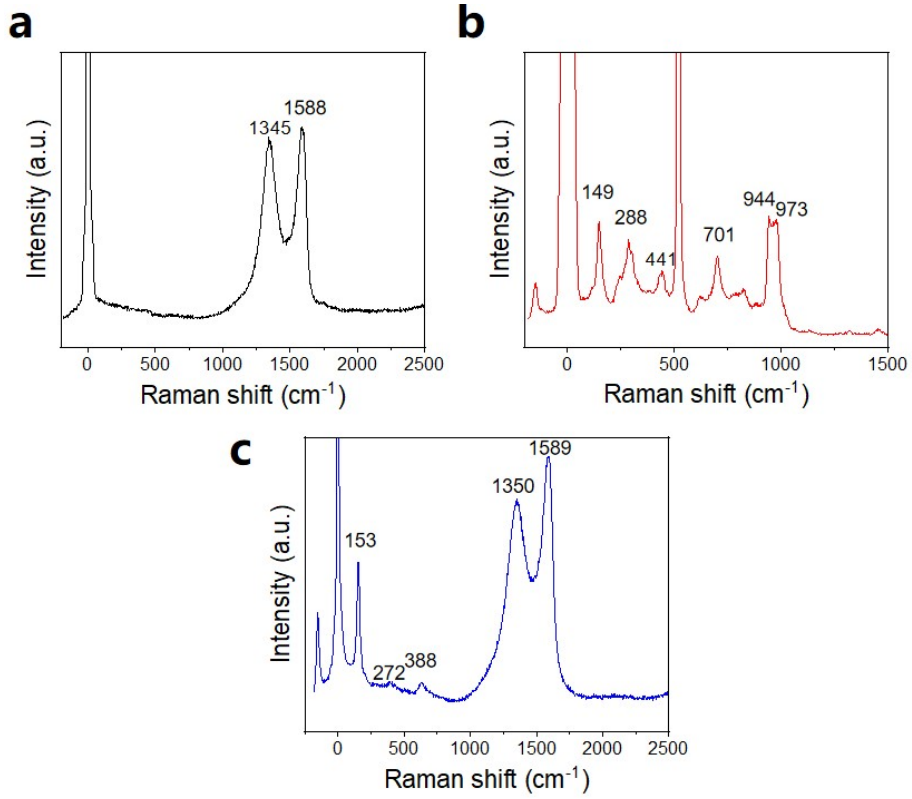

Figure S7. Raman spectra of GO (a), TiO_2 (b) and GO-TiO_2 (c) membranes.

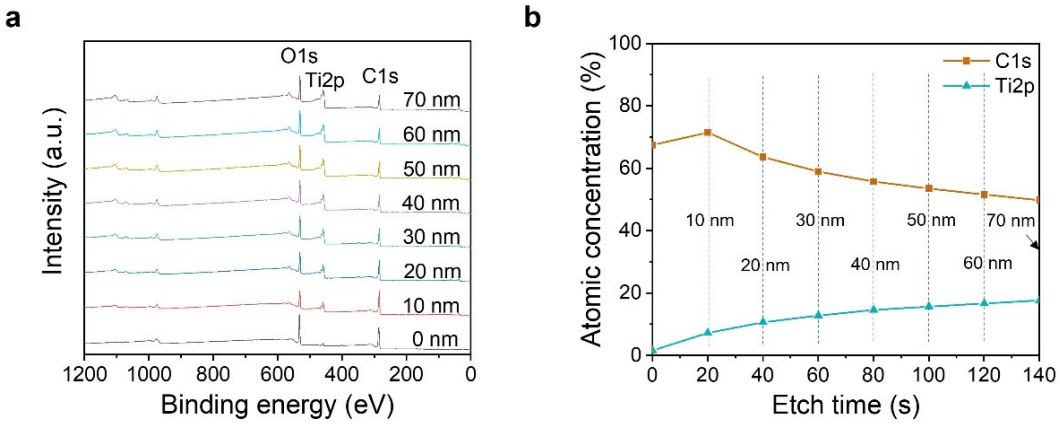

Figure S8. (a,b) XPS depth profile spectra (a) and the corresponding C and Ti atomic concentrations (b). XPS depth profiling shows a GO-rich surface, characterized by a high atomic percentage of carbon and a low percentage of titanium. With increasing etch depth, the carbon content decreases while titanium increases. At 70 nm, the TiO_2: GO mass ratio is approximately 2.5: 1, close to the initial 2.8: 1 feed ratio. Given the membrane's total thickness (> 400 nm), the surface GO enrichment likely results from residual unflocculated GO dispersion before film formation.

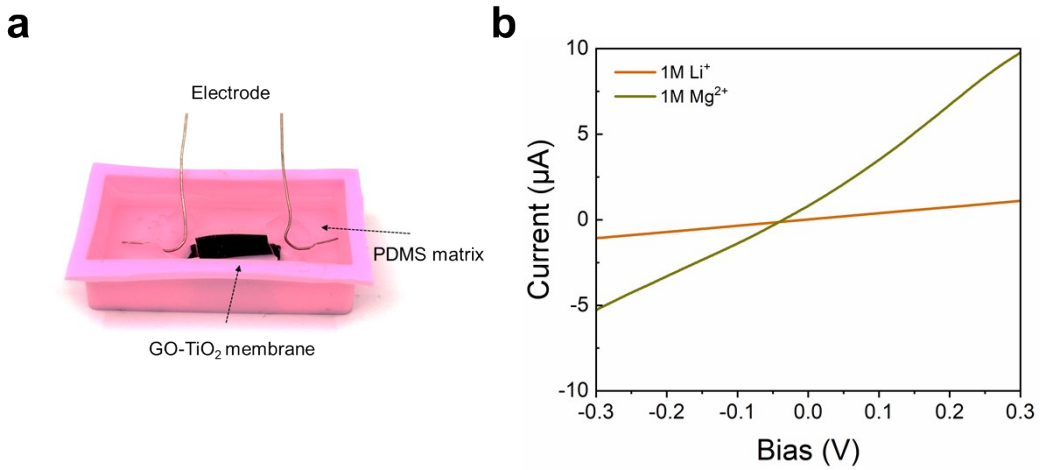

Figure S9. (a,b) Current-voltage (I-V) test of the asymmetric channels of the GO-TiO_2 membrane. The membranes was immersed and sealed salt solution (1 M LiCl or $MgCl_2$), combined with two terminal electrodes (a). Due to the selective ion transport, the obtained I-V curves shows different ionic conductivity. Here, the ionic conductivities of Li^+ and Mg^{2+} are calculated to be 2.2×10^{-2} S m^{-1} and 3.8×10^{-3} S m^{-1}, respectively (b).

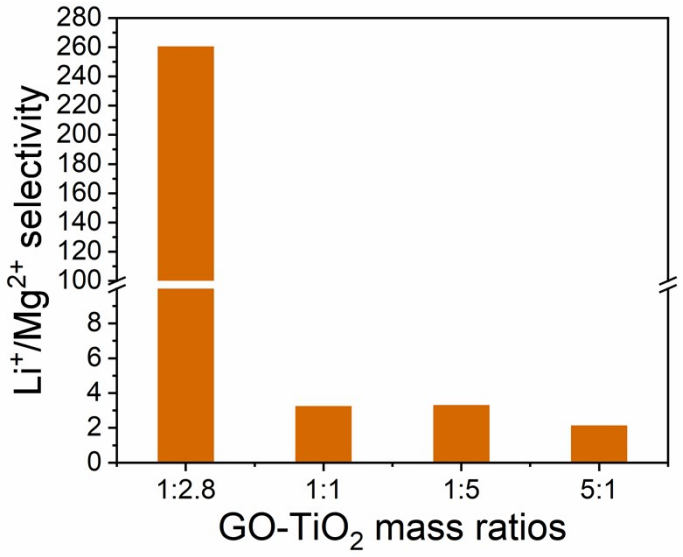

Figure S10. Li^+/Mg^{2+} selectivity of GO-TiO_2 with different mass ratios (GO:TiO_2 = 1:2.8, 1:1, 1:5, 5:1 respectively).

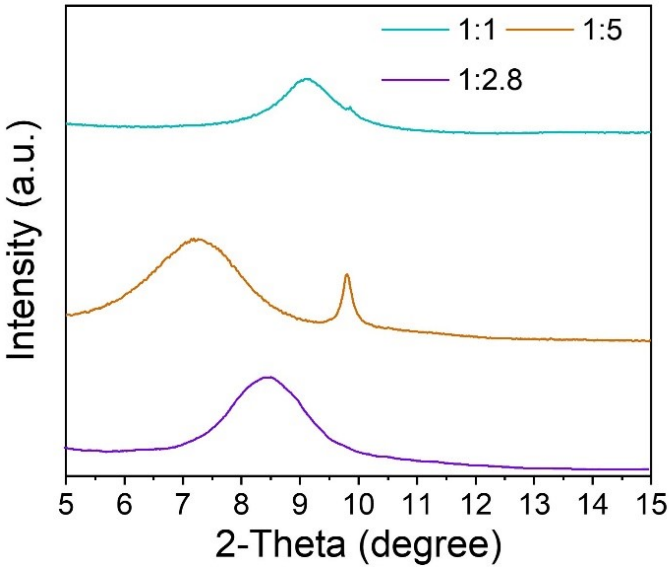

Figure S11. XRD spectra of GO-TiO_2 membranes with different GO: TiO_2 ratio.

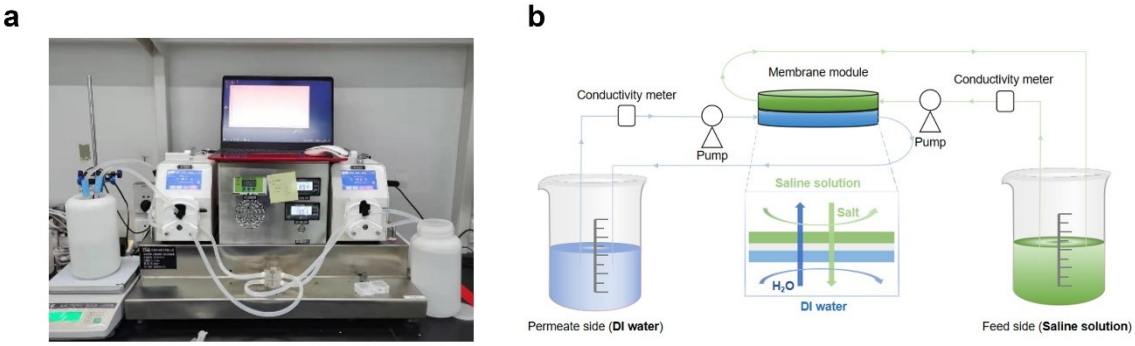

Figure S12. (a,b) Photograph of the forward osmosis setup (a) and corresponding schematic diagram illustrating the principle (b).

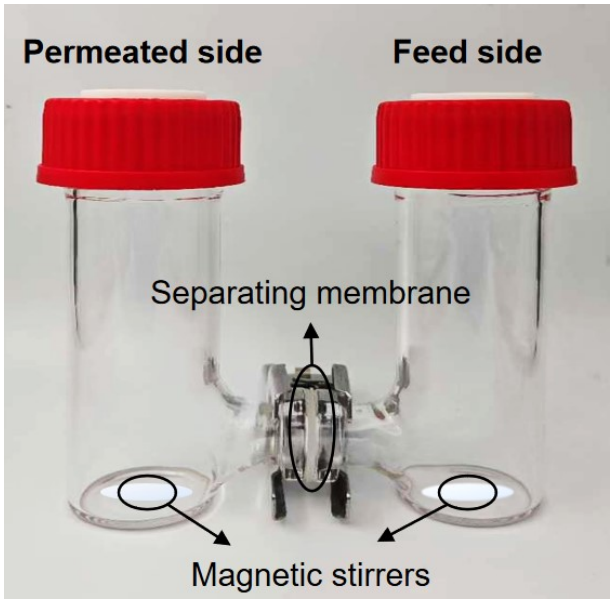

Figure S13. Schematic diagram of the home-made H-type device.

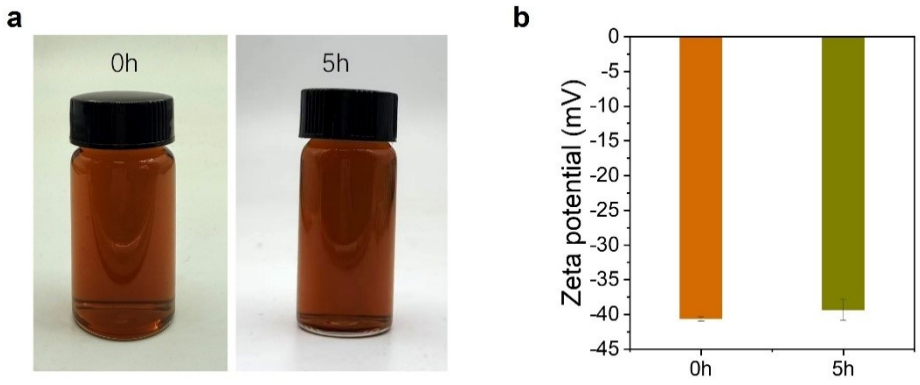

Figure S14. (a) After standing for 5 h, no precipitation can be observed in the mixed GO-MnO_2 solution. (b) Zeta potentials of the mixed GO-MnO_2 solution before and after standing.

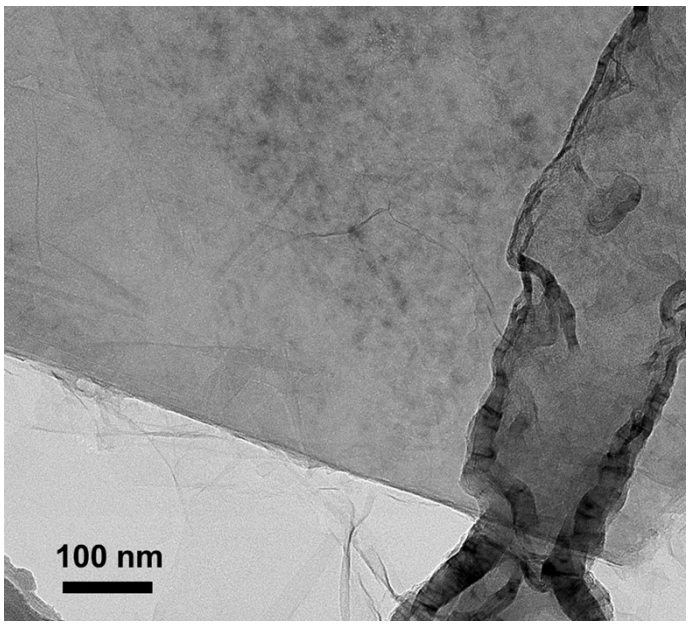

Figure S15. TEM image of exfoliated K-MnO_2 nanosheet

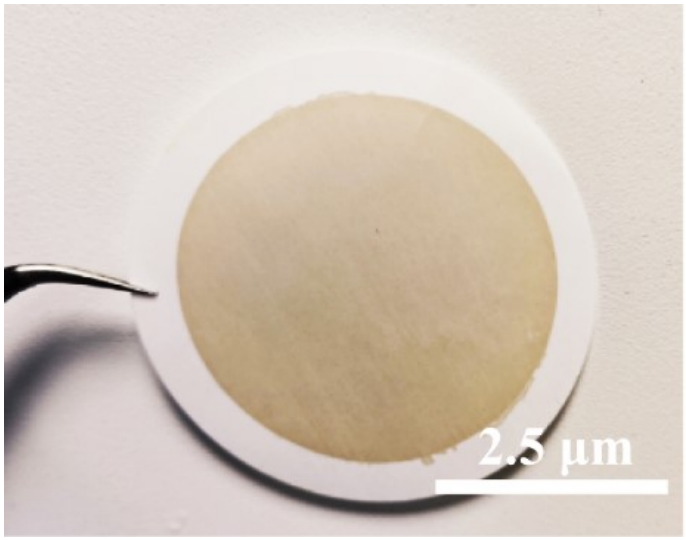

Figure S16. Photo of the prepared GO-MnO_2 membrane

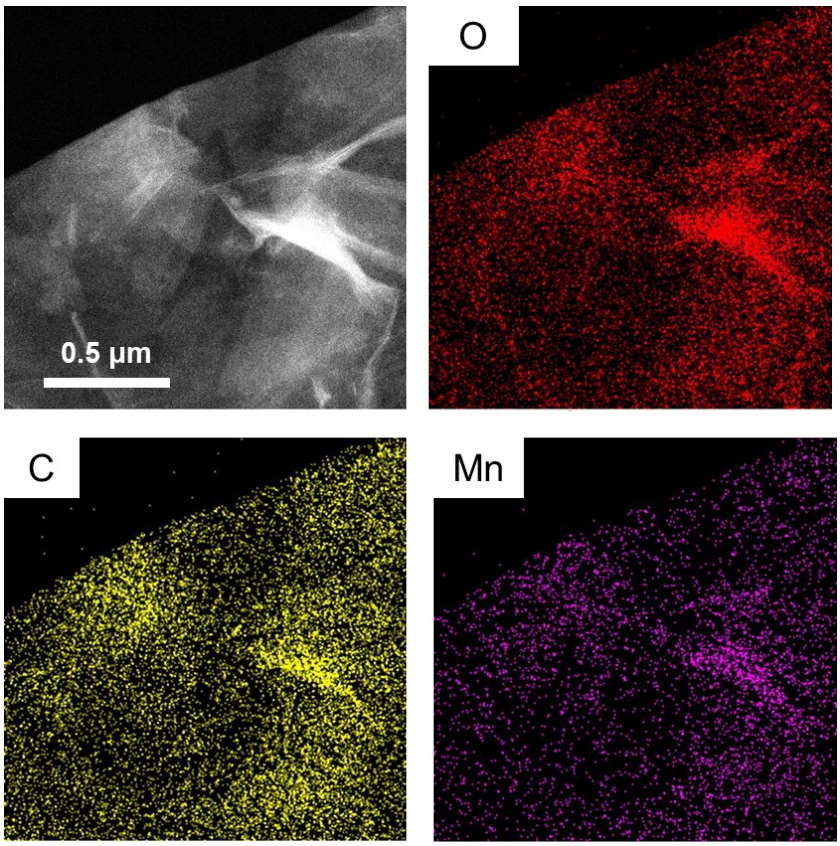

Figure S17. TEM image (top-left) and the corresponding elemental distribution mapping of GO-MnO_2 membrane.

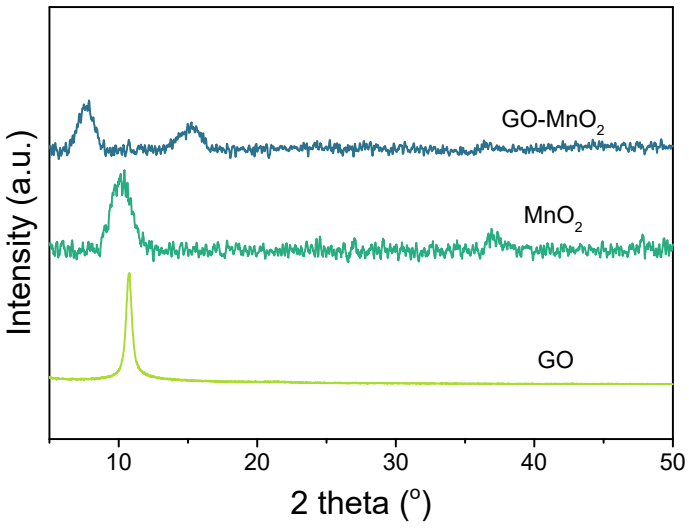

Figure S18. XRD spectra of GO, MnO_2 and GO-MnO_2 membranes. A generated new peak at 7.7° for GO-MnO_2 membrane can be observed.

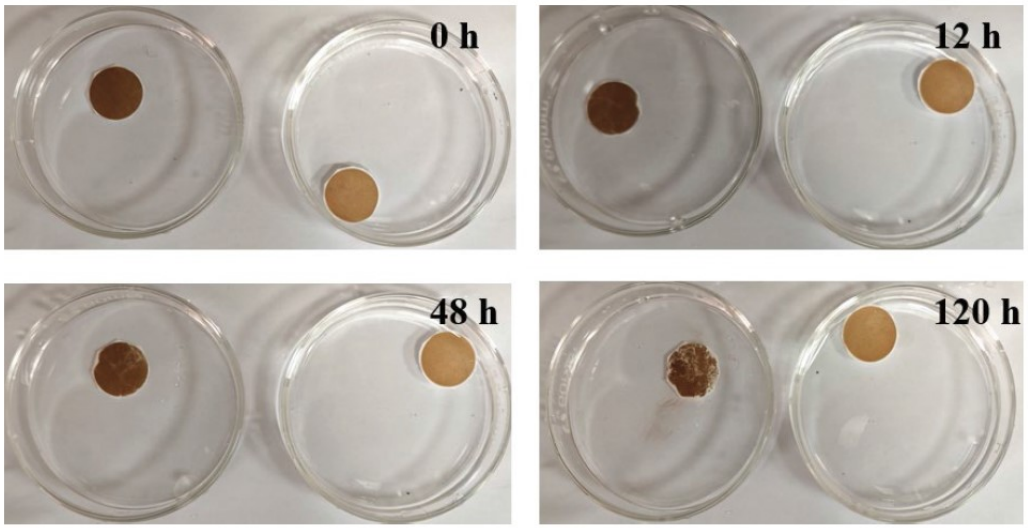

Figure S19. Long-term stability of GO (left) and GO-MnO_2 (right) membranes after immersing in water

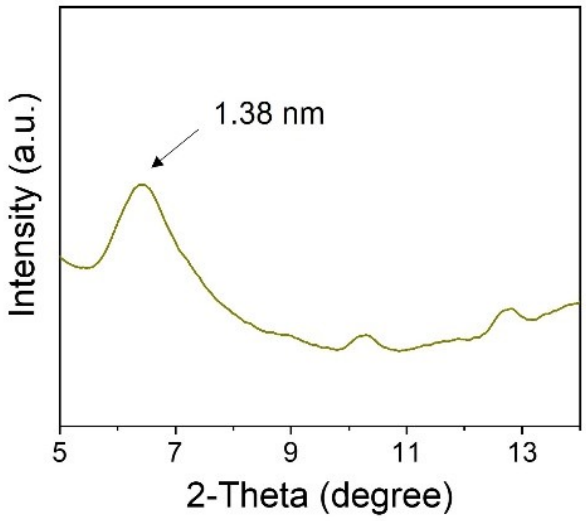

Figure S20. XRD spectrum of wet GO-MnO_2 membrane. Compared with the dry state in Figure 3f, a significant shift in the interlayer *d*-spacing is observed.

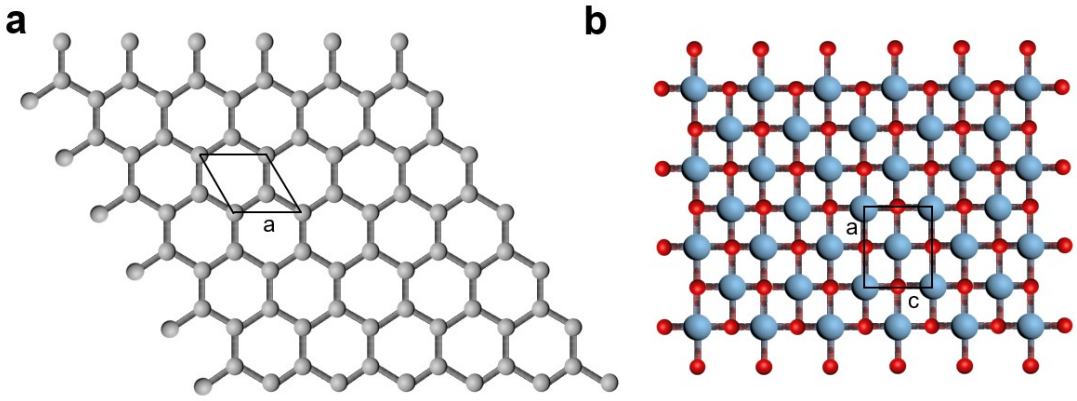

Figure S21. (a) In-plane structure of graphene with a hexagonal unit cell: a = 0.25 nm; (b) In-plane structure of $Ti_{0.87}O_2$ with a rectangular unit cell: a = 0.38 nm, c = 0.30 nm[1]. Through approximate calculations, an ideal graphene structure was utilized in this study to estimate the area balance between GO and $Ti_{0.87}O_2$. The mass surface density of graphene nanosheets is expressed by the formula: $W_{(GO)} = 2M_{(C)}/(a\times a\times \sin 120°\times N_a)$; whereas the mass surface density of $Ti_{0.87}O_2$ nanosheets is given by: $W_{(Ti0.87O2)} = M_{(Ti0.87O2)}/(a\times a\times \sin 120°\times N_a)$. Herein, N_a refers to the Avogadro constant, and $M_{(C)}$ and $M_{(Ti0.87O2)}$ represent the molar masses of C and $Ti_{0.87}O_2$, respectively. Consequently, the mass ratio of $Ti_{0.87}O_2$ to GO is derived as $m_{(Ti0.87O2)}/m_{(GO)} = W_{(Ti0.87O2)}/W_{(GO)} \approx 2.8$.

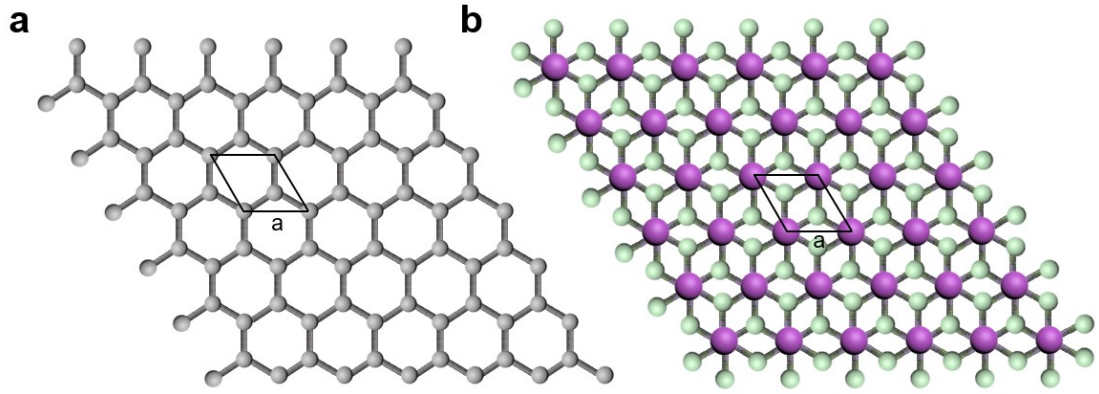

Figure S22. (a) In-plane structure of graphene nanosheets: a = 0.25 nm; (b) In-plane structure of MnO_2 nanosheets: a = 0.28 nm[2]. Through approximate calculations, an ideal graphene structure was adopted in this study to estimate the area balance between GO and MnO_2. The mass surface density of graphene nanosheets is defined by the formula: $W_{(GO)} = 2M_{(C)}/(a\times a\times \sin 120°\times N_a)$; while that of MnO_2 nanosheets is expressed as: $W_{(MnO2)} = M_{(MnO2)}/(a\times a\times \sin 120°\times N_a)$. Herein, N_a denotes the Avogadro constant, and $M_{(C)}$ and $M_{(MnO2)}$ represent the molar masses of C and MnO_2, respectively. Accordingly, the mass ratio of MnO_2 to GO is derived as $m_{(MnO2)}/m_{(GO)} = W_{(MnO2)}/W_{(GO)} \approx 2.5$.

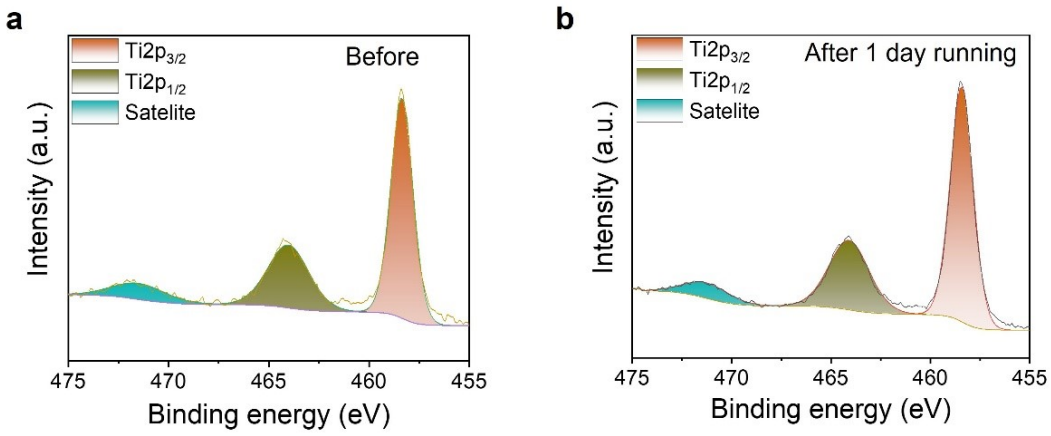

Figure S23. (a,b) XPS spectra of GO-TiO_2 membrane before (a) and after (b) 1 day test of 0.1 M Li^+ permeation.

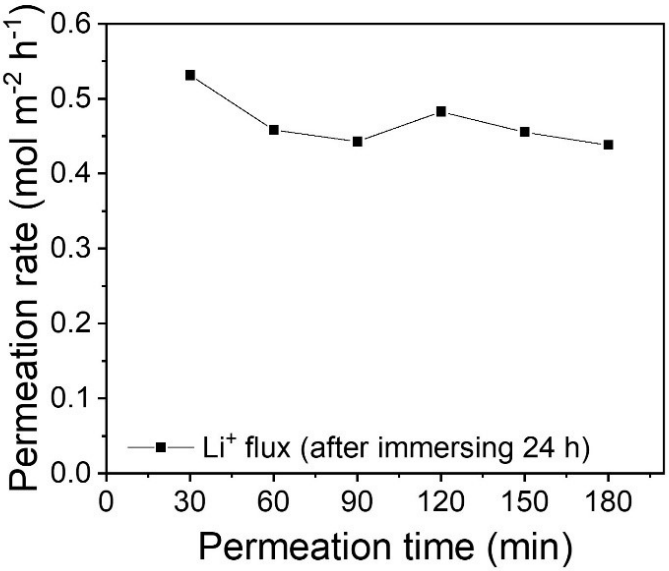

Figure S24. Permeation rate of GO-TiO_2 membrane after immersing in 0.1 M LiCl for 24 h

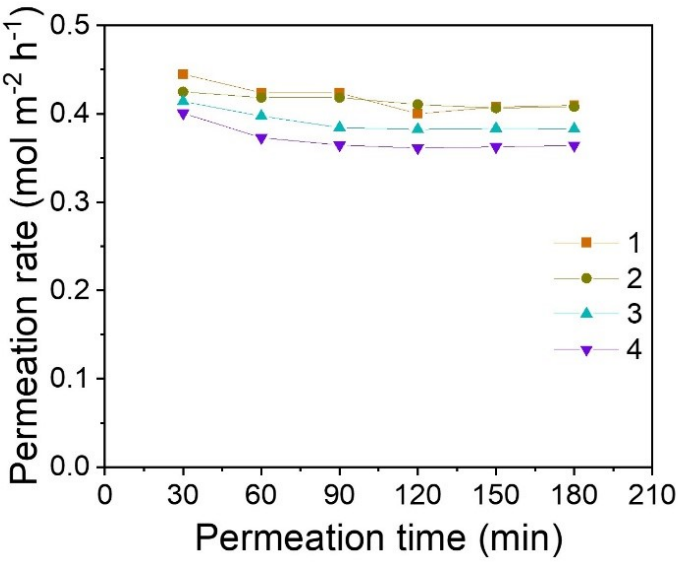

Figure S25. Permeation rate of the GO-TiO_2 membrane over multiple operational cycles. Each cycle consisted of a 180-min filtration period, after which both the feed (brine) and permeate solutions were removed. The system was then replenished with fresh testing solutions to evaluate the impact of loading-unloading cycles on membrane performance.

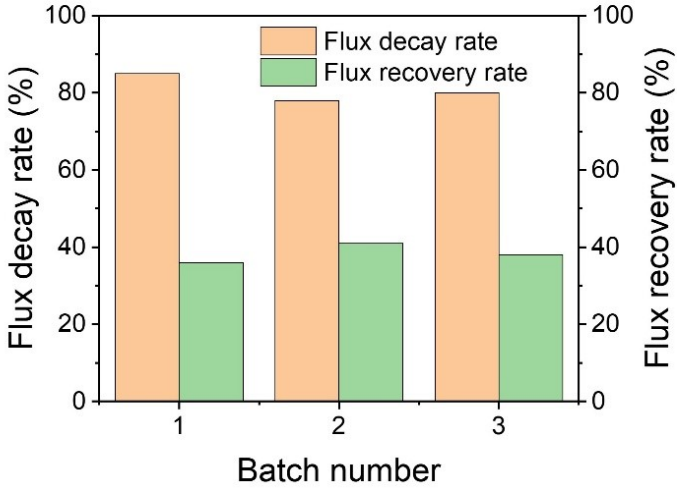

Figure S26. Flux decay rate and flux recovery rate of the GO-TiO_2 membrane after fouling tests. The test procedure was as follows: the membrane was first filtered with pure water to establish the initial water flux, denoted as J_0. Subsequently, a fouling solution was filtered, with the flux recorded as J_p. After fouling, the membrane was rinsed with water, and the pure water flux was measured again, denoted as J_w. The fouling solution consisted of a mixture containing 28 mg/L sodium alginate (SA) and 0.00117 mol/L calcium chloride ($CaCl_2$).

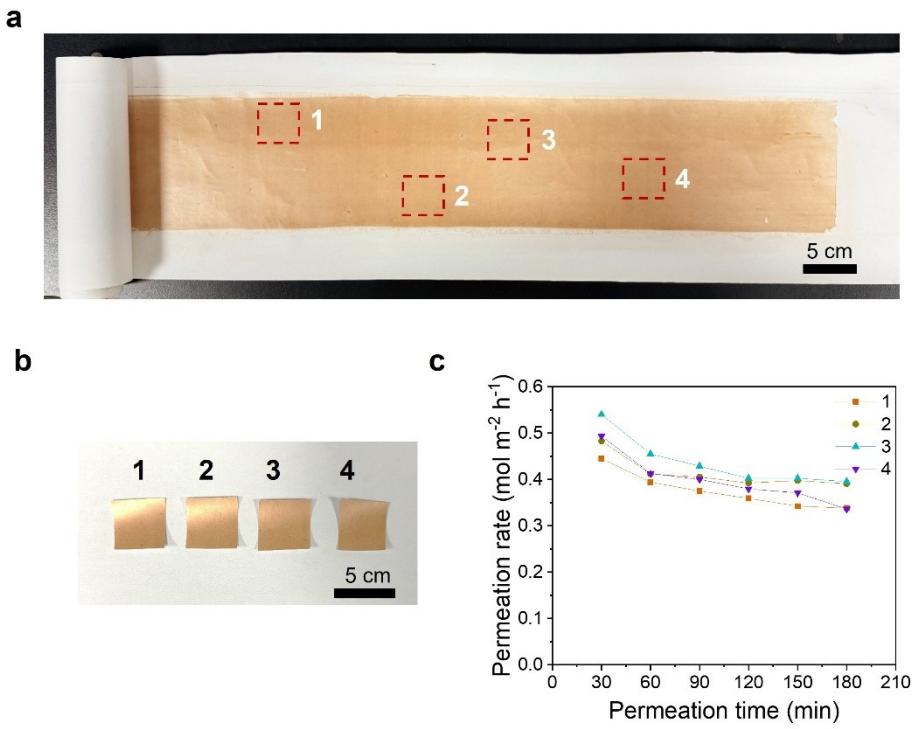

Figure S27. Scalability and uniformity of the GO-TiO_2 membranes. (a) Photo of a large-area membrane prepared via the doctor-blade coating method. (b) Photo of membrane samples harvested from four distinct locations as indicated in (a). (c) Permeation performance of the four corresponding membrane samples tested in a 0.1 M LiCl solution.

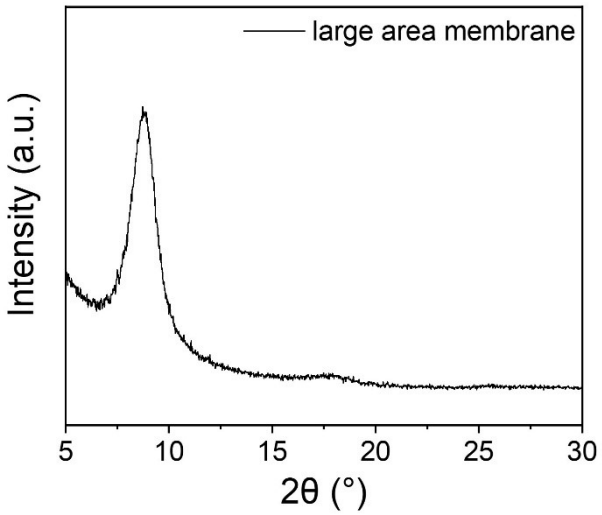

Figure S28. XRD spectrum of large-area GO-TiO_2 membrane prepared via the doctor-blade coating method.

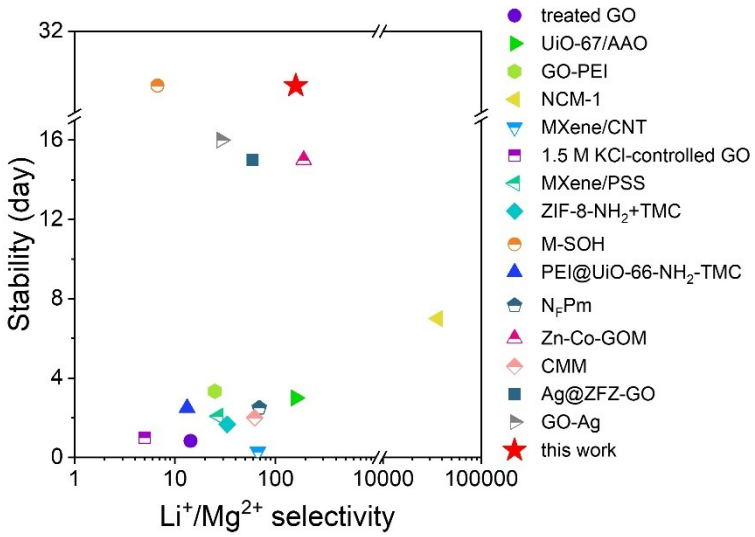

Figure S29. Comparison of Li^+/Mg^{2+} selectivity and stability between this work and other representative membranes including electrically-driven membranes.

Table S1. Comparison of Li^+ permeation rate, Li^+/Mg^{2+} selectivity and stability between this work and other representative membranes.

Membrane	Experimental conditions	Li^+ permeation rate (mol m^{-2} h^{-1})	Li^+/Mg^{2+} selectivity	Membrane stability	References
treated GO	mixed solution of 0.1 M LiCl and 0.1 M $MgCl_2$	~0.18	14.3	0.833	J. Ma, *J. Phys.: Conf. Ser.* **2025**, 3092, 012004.
GO-PEI	single-salt system (0.5 M LiCl or 0.5 M $MgCl_2$)	＜0.05	~25	3.33	W. Zhang, Q. Huang, S. Liu, M. Zhang, G. Liu, Z. Ma, W. Jin, *Sep. Purif. Technol.* **2022**, 291, 120938.
1.5 M KCl-controlled GO	single-salt system (0.1 M LiCl or 0.1 M $MgCl_2$)	0.32	~5	1	S. Liang, S. Wang, L. Chen, H. Fang, *Sep. Purif. Technol.* **2020**, 241, 116738.
MXene/PSS	single-salt system (0.2 M LiCl or 0.2 M $MgCl_2$)	0.08	27	2.08	Z. Lu, Y. Wu, L. Ding, Y. Wei, H. Wang, *Angew. Chem. Int. Ed.* **2021**, 60, 22265-22269.
ZIF-8-NH_2+TMC	single-salt system (0.1 M LiCl or 0.1 M $MgCl_2$)	0.863	33.06	1.67	H. Jia, Y. Wang, L. Yang, R. Fang, *Sep. Purif. Technol.* **2025**, 362, 131870.
M-SOH	single-salt system (0.1 M LiCl or M $MgCl_2$)	7.4×10^{-5}	6.7	30	H. Peng, Y. Hu, S. Li, J. Rao, Q. Zhao, *J. Membr. Sci.* **2023**, 674, 121515.
PEI@UiO-66-NH_2-TMC	single-salt system (0.1 M LiCl or 0.1 M $MgCl_2$)	0.68	13.2	2.5	X. Cui, G. Kong, S. Wei, Y. Cui, P. Yu, Z. Kang, H. Guo, *Sep. Purif. Technol.* **2024**, 330, 125485.
N_FPm	2000 ppm, Mg^{2+}/Li^+ of 20, 6 bar	--	69	2.5	Y. Yang, Y. Zhao, S. Zhao, R. Yao, H. Li, J. Ma, C. Shi, S. Bai, X. Wang, J. Li, X. Feng, B. Wang, *ACS Nano*. **2026**, 20, 2064-2072.

Zn-Co-GOM	K^+ 2.61 g/L, Na^+ 44.24 g/L, Li^+ 0.19 g/L, Mg^{2+} 0.36 g/L, PH=4	--	191.13	15	F. Yuan, Q. Gao, Z. Lv, Y. Zhang, X. Liu, J. Peng, Z. Li, *Nano Lett.* **2024**, 24, 14346-14354.
CMM	mixed solution of 0.5 M $MgCl_2$ and 30 mM LiCl	0.059	62	2	G. Zhang, G. Hu, J. Li, G. Feng, Y. Cui, Z. Chen, Z. Liu, Y. Cui, *Proc. Natl. Acad. Sci. U.S.A.* **2025**, 122, e2511666122.
Ag@ZFZ-GO	K^+ 2.61 g/L, Na^+ 44.24 g/L, Li^+ 0.19 g/L, Mg^{2+} 0.36 g/L, PH=4	--	59.3	15	Y. Hao, X. Liu, Y. Zhang, X. Zhang, Z. Li, X. Chen, *Adv. Sci.* **2024**, 11, 2406535.
GO-Ag	K^+ 2.61 g/L, Na^+ 44.24 g/L, Li^+ 0.19 g/L, Mg^{2+} 0.36 g/L, PH=7	--	29	16	Y. Yang, Q. Gao, W. Liang, X. Zhang, L. Qian, Z. Li, X. Chen, *Small*. **2025**, 21, 2409950.
NCM-1	(Electrically-driven) single-salt system (0.1 M LiCl or 0.1 M $MgCl_2$),	~0.58	36161.7	7	F. Fan, Y. Ren, S. Zhang, Z. Tang, J. Wang, X. Han, Y. Yang, G. Lu, Y. Zhang, L. Chen, Z. Wang, K. Zhang, J. Gao, J. Zhao, G. Cui, B. *Tang, Adv. Sci.* **2024**, 11, 2402898.
MXene/CNT	(Electrically-driven) single-salt system (0.1 M LiCl or 0.1 M $MgCl_2$)	0.229	67	7	J. Lu, C. Dai, S. Li, D. Zou, Y. Sun, W. Jing, *Sep. Purif. Technol.* **2024**, 338, 126508.
UiO-67/AAO	(Electrically-driven) single-salt system (0.1 M LiCl or 0.1 M $MgCl_2$)	27	159.4	3	R. Xu, Y. Kang, W. Zhang, X. Zhang, B. Pan, *Angew. Chem. Int. Ed.* **2022**, 61, e202115443.
GO-TiO_2		**~0.4**	**159.7**	**30**	**This work**

References

[1] Pan X.; Fan Z.; Zhang X.; Liu Y.; Wu Y.; Wang S.; Safaei J.; Sun B.; Ma R.; Liu Z.; Bando Y.; Sasaki T.; Wang X.; Zhu J.; Wang G. Atomic-scale regulation of anionic and cationic migration in alkali metal batteries. *Nat. Commum.* **2021**, *12*, 4184.

[2] Xiong P.; Ma R.; Sakai N.; Sasaki T. Genuine unilamellar metal oxide nanosheets confined in a superlattice-like structure for superior energy storage. *ACS Nano* **2018**, *12*, 1768-1777.